



**The Abdus Salam
International Centre for Theoretical Physics**



2245-16

**Joint ICTP-IAEA Advanced School on the Role of Nuclear Technology
in Hydrogen-Based Energy Systems**

13 - 18 June 2011

Comparative review of atomic and (magnetic) ordering in intermetallics

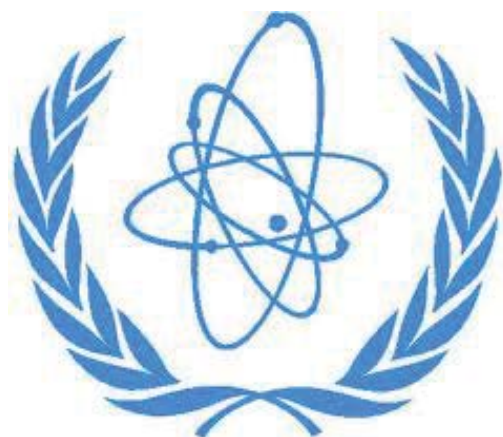
Daniel Fruchart
*Institut Neel, CNRS
Grenoble
France*

Comparative review of atomic and (magnetic) ordering in intermetallics using various scale probes such as neutron scattering, Mössbauer, μ^+ SR, PAC, XANES-EXAFS-XMCD and NMR spectroscopies

Daniel Fruchart

Institut Néel, CNRS, BP 166, 38042, Grenoble Cedex 9, France

**Joint ICTP-IAEA School
on the Role of Nuclear Technologies
In Hydrogen-Based Energy Systems**



Guideline

Metal hydrides are expected to play a unique role in opening specific solutions for future reversible energy storage systems from very large to intermediate scales up to integrated devices, for both stationary and mobile applications.

However, magnetic and electronic aspects of certain materials will play key role in capture the renewable energies :

Strong magnets for wind-mills, sensors...

Magnetocalorics for refrigeration...

Thermo-electrics, photo-voltaic

Also ageing and corrosion have to be probed.

Most of nuclear based technologies are well adapted to investigated and probe both storage and ancillaries solid state materials

Introduction

The intrinsic and extrinsic properties of many (magnetic) compounds having potentially high applied properties (hard magnets, very soft materials, magnetostrictive and magnetocaloric materials, alloys forming hydrides...) must be probed at different scales in their characteristics, e.g. bulk to atomic and to orbital parameters.

Scales

Bulk (mm to cm)... actuators,	Optic transducers, magnetostrictive
Micrometric (1 to 10 μm)...	soft magnetic circuits Magnetic domains
Mesometric (nm to 1 μm)...	Bits for magnetic recording
Nanometric (1 to 10 nm)...	Magneto-optics films and layers

What scale to probe? A tutorial example :

A modern magnet is a cm-piece of hard magnetic material

e.g. : Nd-Fe-B \Rightarrow Nd₂Fe₁₄B + Nd₂₀Fe₂₀ + ... \Rightarrow Nd₁₅Fe₇₇B₈

Nd-Fe-B + H₂ \Rightarrow Nd₂Fe₁₄BH_{5.5} low temperature

Nd-Fe-B + H₂ \Rightarrow NdH_{2.2} + Fe + Fe₂B high temperature

few cm = size of a magnet \Rightarrow magnetic induction at cm to 10 cm

Devices = electrotechnique, neutronographie

10 to 100 μm = size of grains \Rightarrow process : pressing, orienting...

Corrosion process = X-ray and nuclear neutron diffraction, EXAFS, SEM

1 to 10 μm = size of crystallites \Rightarrow chemistry = phase equilibrium, anisotropy of texture...

Mechanical properties (ductile, fragile), magnetisation, SEM

0.1 to 5 μm = size of domains \Rightarrow coercivity

Micromagnetics, MOKE, XMCD-PEEM, TEM

few nm to μm = intergrain size and interfaces

Neutron diffraction, ss NMR, XANES, EXAFS, SANS, TEM, AFM

0.1 to 0.3 nm size of atoms and coordination distances

Neutron scattering, ^{57}Fe Mössbauer, μ^+ SR, PAC, EXAFS, XMCD and NMR spectroscopies, AFM

The best knowledge is gained when one is able to anticipate the behaviour of optimised formula and the quality of the related micro- to nano- structure by using panels of complementary techniques. It is interesting to compare the respective advantages and merits of the different probing method reference to their scales....

Review

Atomic to sub atomic scale analysis = physics-chemistry of materials

Magnetism in Fe-based intermetallics: relationships between local environments and local magnetic moments

Daniel Fruchart

Laboratoire de Cristallographie du C.N.R.S., associé à l'Université J. Fourier, BP 166, 38042 Grenoble, Cedex 9 (France)

(Received August 5, 1993)

Abstract

We report on the relationship between the local magnetic moments and crystal sites, mainly in iron-rich intermetallics. The topology of the atomic environment is analysed in terms of numbers of neighbours, disclination lines and atomic domains. The wide range of compounds studied includes rare earth-iron alloys, such as R_6Fe_{23} , RFe_3 , $R(FeM)_{12}$, R_2Fe_{17} , ternary rare earth-iron-metalloid intermetallics such as $R_2Fe_{17}H_x$, $R_2Fe_{17}N_3$, $R_2Fe_{17}C_x$, $R_2Fe_{14}B$, $ThFe_{11}C_x$, $R(FeM)_{12}N_x$ and $R(FeM)_{12}C_x$, as well as binary iron nitrides (Fe_3N , Fe_4N , $Fe_{16}N_2$), carbides (Fe_5C_2 , Fe_3C) or borides (Fe_2B and Fe_3B).

The sites having major ligand lines are observed to carry the larger magnetic moments encountered in the structures. In the ternary compounds strong bonds are found between iron sites and a neighbouring metalloid atom, thus leading to a lower iron magnetic moment. Finally, a close relationship between the local moment and the volume of the iron site has been observed: a large atomic domain is found to favour a high moment.

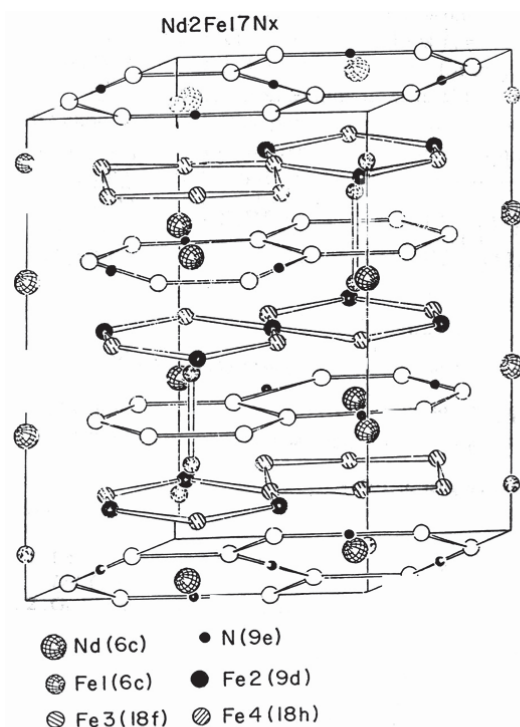


Fig. 1. Schematic representation of the Nd₂Fe₁₇N₃ rhombohedral structure. In the hexagonal representation the 4f, 6g, 12j and 12k crystal sites respectively correspond to 6c, 9d, 18f and 18h as described in the rhombohedral symmetry.

TABLE 2. Local coordinations and atomic cell volumes in Nd₂Fe₁₇N_x and in Pr₂Fe₁₇N_x.

(a) Nd ₂ Fe ₁₇ N _x (S.G.: R $\bar{3}$ m)	Nd (6c)	Fe (6c)	Fe (9d)	Fe (18f)	Fe (18h)	N (9e)
$x=0.0$ [22]						
W.S. ^a (Å ³)	31.74	12.29	11.25	11.73	12.09	—
$x=2.6$ [86]						
W.S. ^a (Å ³)	31.96	12.82	11.88	11.74	12.39	3.67
$x=2.7$ [36]						
W.S. ^a (Å ³)	32.10	12.76	11.84	11.75	12.43	3.75
$x=3.0$ [20]						
W.S. ^a (Å ³)	32.20	12.76	11.92	11.76	12.49	3.76
$\Delta(\text{W.S.})/(\text{W.S.}) (\times 10^3)$	14.5	38.2	59.5	2.5	33.1	—
$d(\text{Fe-N})$ (Å)	—	3.97	3.30	1.92	1.94	—
$M(\text{Fe})$ (μ_B) [20]	—	3.2(2)	2.4(2)	2.2(2)	1.9(1)	—
$h.f.(\text{Fe})$ (kOe) [24] ^b	—	370	340	312	290	—
(b) Pr ₂ Fe ₁₇ N _x (S.G.: R $\bar{3}$ m)	Pr (6c)	Fe (6c)	Fe (9d)	Fe (18f)	Fe (18h)	N (9e)
$x=0.0$ [18]						
W.S. ^a (Å ³)	31.79	12.28	11.22	11.76	12.13	—
$x=3.0$ [18]						
W.S. ^a (Å ³)	32.04	12.69	11.76	11.70	12.40	3.71
$\Delta(\text{W.S.})/(\text{W.S.}) (\times 10^3)$	7.9	33.4	48.1	-5.0	22.3	—
$d(\text{Fe-N})$ (Å)	—	3.93	3.29	1.91	1.94	—
$M(\text{Fe})^c$ (μ_B) [20]	—	2.9(2)	2.3(2)	1.9(2)	1.7(1)	—

^aWigner-Seitz atomic cell volume as calculated from ref. 66 using $r_{\text{Nd}}=1.82$ Å, $r_{\text{Pr}}=1.82$ Å, $r_{\text{Fe}}=1.26$ Å and $r_{\text{N}}=0.92$ Å.

^bValues determined for Y₂Fe₁₇N₃.

^cThe magnetic moment values are those determined for the isotope compound Ce₂Fe₁₇N₃ for which the structure parameters are almost identical.

About techniques : allow analyse and understand parameters at

§ **micrometric scale**

§ **nanometric scale**

§ **atomic scale**

§ **orbital scale**

Static atom ordering (from crystal, defects to glasses)

Chemical bonding (coordination, distances, electronic state...)

Magnetic atom ordering (coupling forces and magnetic local polarisation)

Dynamics of atoms, interstitials and molecules

Chemical reactivity (bonding, surface, catalysts...)

Dynamics

Techniques	Targets	Probes	Parameters
Magnetisation Suceptibility	electrons (s, p, d, f)	magnetic electrons	moments couplings
X-ray scattering	full electron density	electron	atom ordering
EXAFS	photo-electron absorption	n. neighbour atom coordin.	atom ordering
XANES	photo-electron absorption	orbital overlaps	electronic state, bonds
XMCD	photo-electron magnet. absorption	magnetically polarised trans.	spin & orbit components crystal-field
Magnetic neutron scattering	polarised electrons	spin density (static–dyn.)	magnetic orderings & couplings crystal-field
μ^+SR	muon (big electr.) positron annilat.	electron density (static–dyn.) muoniun	magnetism diffusion bonds

Techniques**Targets****Probes****Parameters**

**Nuclear neutron
scattering
absorption**

**nucleus n°
interaction
absorption**

**static nucleus
atom dynamics
neutronography**

**atom order.
proton diff.**

**Mössbauer
(Fe, Sn, RE)
(synchrotron)**

**nucleus
transition**

**electron
density
polarisation**

**moments
electro. state
electric field**

**PAC
(Hf...)
(synchrotron)**

**nucleus
transition**

**electron
density
polarisation**

**moments
electro. state
electric field**

ss NMR

**nucleus spin
spectroscopy**

**electron
density
polarisation**

**moments
electro. state
electric field
diffusion
dynamics**

**EPR
IR, Raman...
Compton
Annihilation...**

Short review on principles

Interaction of neutrons with matter

	elastic scattering	inelastic scattering
strong-force interaction ("nuclear scattering")	position of nuclei in solid (lattice structure)	lattice vibrations (phonons)
magnetic interaction	position and orientation of electronic magnetic moments in solids (ferromagnetism, antiferromagnetism)	spin excitations (magnons, spin waves)

Diffuse amplitude given by :

$$f_N(\mathbf{k}, \mathbf{k}_0) = -m/2\pi\hbar^2 \int V(\mathbf{r}) \exp -2\pi (\mathbf{H} \cdot \mathbf{r}) d^3r$$

$$\mathbf{Q} = \mathbf{k} - \mathbf{k}_0 \text{ wave vectors}$$

nuclear potential $V(\mathbf{r})$ is extremely short distance active

diffuse nuclear amplitude of isolated atom (nucleus) is independent of q

neutron ($S = 1/2$) scattering with nucleus (I) leads to 2 states

$a^+ = I + 1/2$ and $a^- = I - 1/2$ of respective population $2I + 2$ and $2I$

So coherent cross sections are defined :

Coherent
$$b_C = a^+(I + 1) / (2I + 1) + a^-(I) / (2I + 1)$$

Incoherent
$$B_I = (a^+ + a^-) / (2I + 1) \quad (\text{indep. on } H)$$

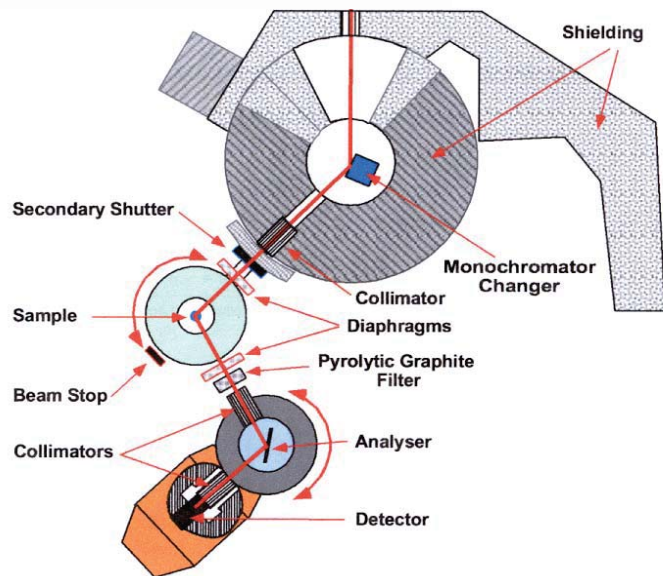
dipolar potential for **magnetic** scattering

$$f_M(\mathbf{k}, \mathbf{k}_0) = 2m/h^2 (\mathbf{M}_N \times \mathbf{e}) \cdot (\mathbf{M}_{el} \times \mathbf{e}) \sim \gamma e^2 / (m_0 c^2) S_N \cdot S_{el\perp} f_{el}(H)$$

Double differential coherent and incoherent diffusion cross sections

$$\left(\frac{d^2\sigma}{d\Omega dE}\right)_{\text{coh}} = \frac{k}{k_0} \frac{1}{2\pi\hbar N} \int \exp(-i\omega t) dt \sum_i^N \sum_j^N b_i b_j^* \cdot \langle \exp[-i\vec{Q}\cdot\vec{r}_j(0)] \exp[i\vec{Q}\cdot\vec{r}_i(t)] \rangle$$

$$\left(\frac{d^2\sigma}{d\Omega dE}\right)_{\text{inc}} = \frac{k}{k_0} \frac{1}{2\pi\hbar N} \int \exp(-i\omega t) dt \sum_j^N \overline{b_j^2} \text{incoh} \cdot \langle \exp[-i\vec{Q}\cdot\vec{r}_i(0)] \exp[i\vec{Q}\cdot\vec{r}_i(t)] \rangle$$



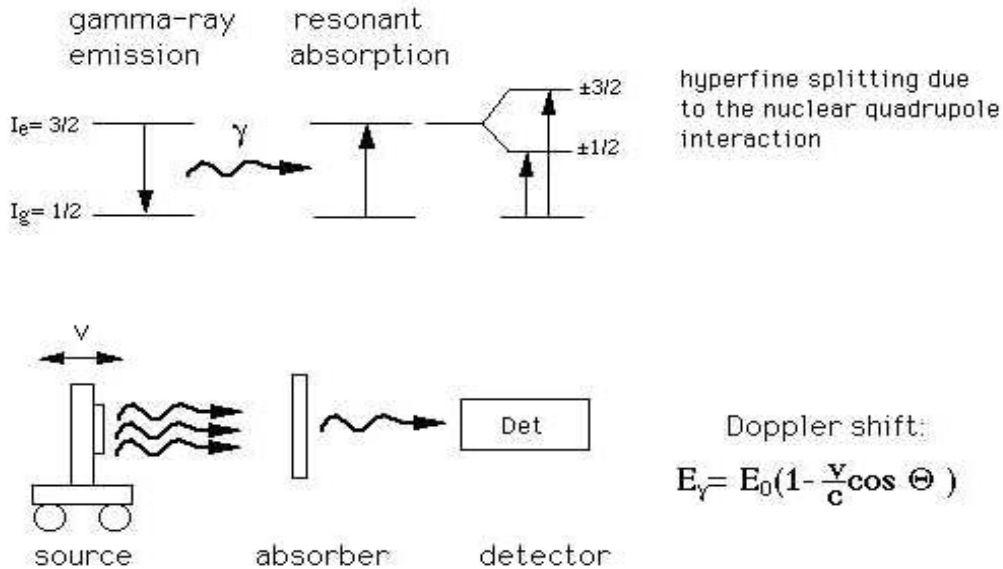
Quasi elastic neutron scattering

$$S_s^{\text{qe}}(\vec{Q}, \omega) = \exp[-\langle u^2 \rangle Q^2] \cdot \frac{1}{\pi} \frac{DQ^2}{[DQ^2]^2 + \omega^2}$$

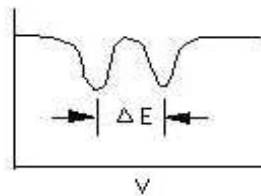
→ Chudley-Elliot model

Mossbauer effect (ME)

(recoilless gamma-ray emission and absorption)



For low-energy gamma rays ($E < 50$ keV), there is a significant probability that the emission and absorption events are recoilless, meaning that no phonons are created or destroyed. Then, the emission and absorption profiles have a width given only by the lifetime uncertainty. For a typical lifetime of 100 nanoseconds, the energy uncertainty is only about 1 nano-electron-volt, small enough to permit resolution of hyperfine energy splittings of the excited and ground nuclear states.



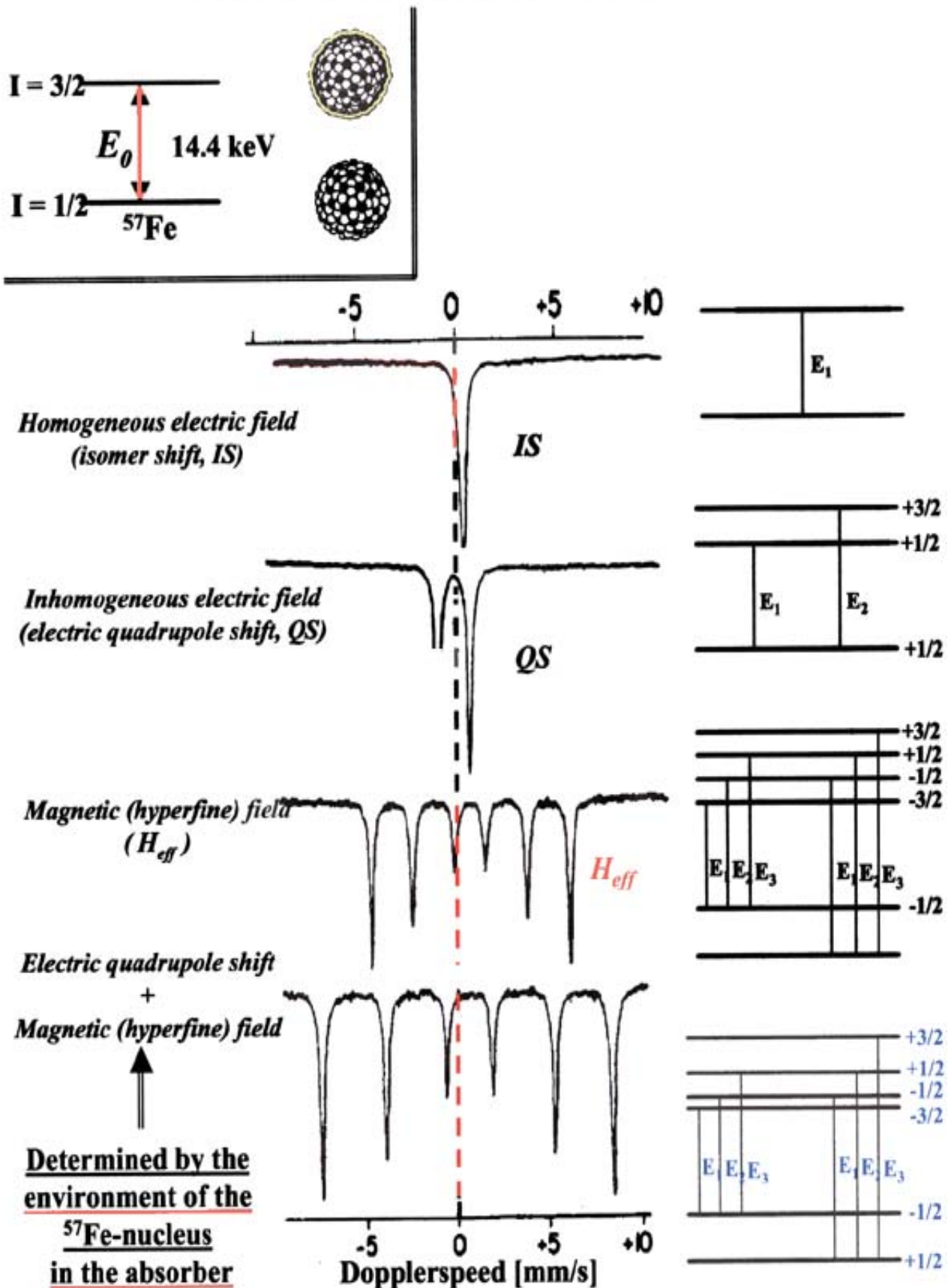
Transmission spectrum: Splittings arise from the interactions of nuclear moments with internal fields in solids.

$v \sim 1 \text{ cm/s}$

$\Delta E \sim 10^{-6} \text{ eV} \sim 100 \text{ MHz}$

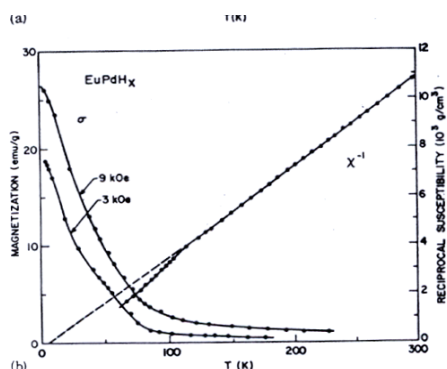
H																	He
Li	Be											B	C	N	O	F	Ne
Na	Mg											Al	Si	P	S	Cl	Ar
K	Ca	Sc	Ti	V	Cr	Mn	Fe	Co	Ni	Cu	Zn	Ga	Ge	As	Se	Br	Kr
Rb	Sr	Y	Zr	Nb	Mo	Tc	Ru	Rh	Pd	Ag	Cd	In	Sn	Sb	Te	I	Xe
Cs	Ba	La	Hf	Ta	W	Re	Os	Ir	Pt	Au	Hg	Tl	Pb	Bi	Po	At	Rn
Fr	Ra	Ac															
		Ce	Pr	Nd	Pm	Sm	Eu	Gd	Tb	Dy	Ho	Er	Tm	Yb	Lu		
		Th	Pa	U	Np	Pu	Am	Cm	Bk	Cf	Es	Fm	Md	No	Lr		

Mössbauer spectroscopy

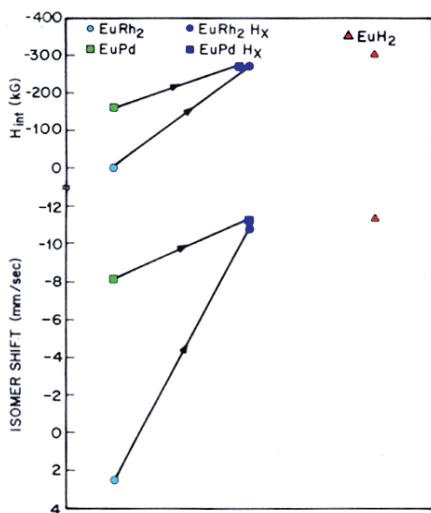


Applications

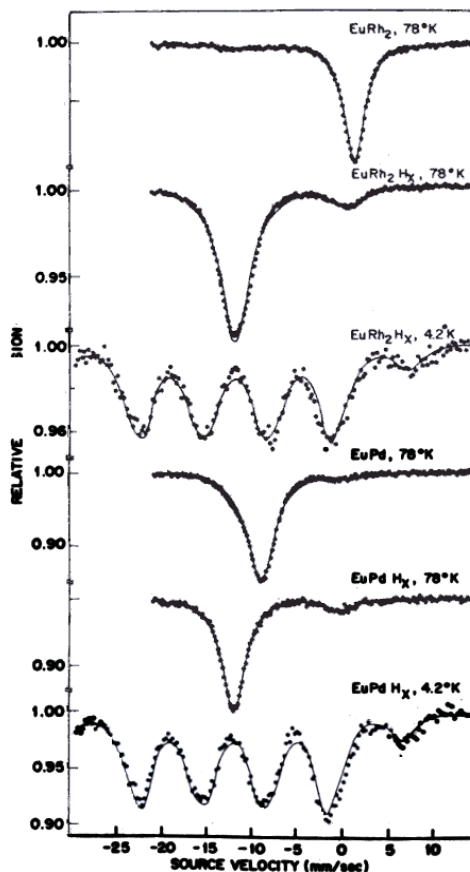
EuRh₂, EuPd₂
 → **heat of formation**
of their hydrides



(a) Temperature dependence of the magnetization (σ) and the reciprocal susceptibility (χ^{-1}) of EuRh₂ after hydrogen absorption. (b) Temperature dependence of the magnetization (σ) and the reciprocal susceptibility (χ^{-1}) of EuPd after hydrogen absorption.



Changes in isomer shift and hyperfine field splitting due to hydrogen absorption into EuRh₂ and EuPd, and corresponding EuH₂ values.



Eu¹⁵¹ Mössbauer spectra of EuRh₂ and EuPd before and after hydrogen absorption.

$$\Delta H(\text{GdRh}_2\text{H}_x) = \Delta H(\text{GdH}_2) + \Delta H(\text{Rh}_2\text{H}_{2-x}) - \Delta H(\text{GdRh}_2), \quad 1$$

$$\Delta H(\text{Eu}^{\text{III}}\text{Rh}_2\text{H}_x) = \Delta H(\text{Eu}^{\text{III}}\text{H}_2) + \Delta H(\text{Rh}_2\text{H}_{2-x}) - \Delta H(\text{Eu}^{\text{III}}\text{Rh}_2), \quad 2$$

$$\Delta H(\text{Eu}^{\text{II}}\text{Rh}_2\text{H}_x) = \Delta H(\text{Eu}^{\text{II}}\text{H}_2) + \Delta H(\text{Rh}_2\text{H}_{2-x}) - \Delta H(\text{Eu}^{\text{III}}\text{Rh}_2). \quad 3$$

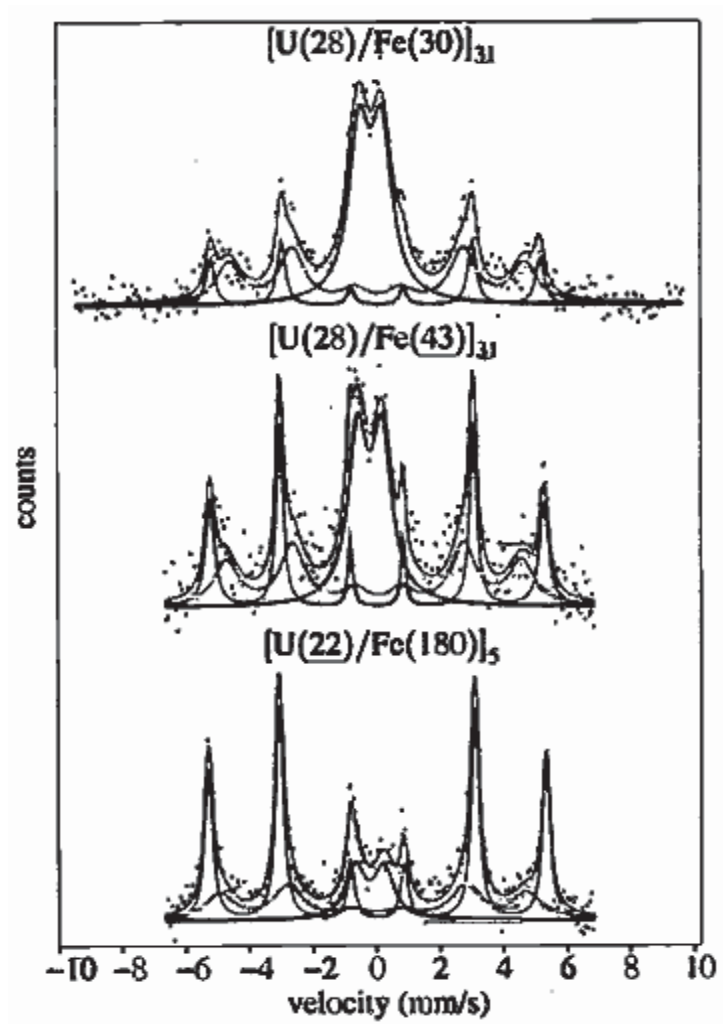
TABLE II. Values of the heat of formation terms appearing in Eqs. (1), (2), and (3).

$\Delta H(\text{RRh}_2\text{H}_2)$	$\Delta H(\text{RH}_2)$	$\Delta H(\text{Rh}_2\text{H}_2)$	$-0.7 \Delta H(\text{RRH}_2)$	Eq.
-3, 5(-1, 4)	-54	+13, 4	0.7×53	1
+3, 4(+1, 4)	-31	+13, 4	0.7×30	2
-5, 2(-2, 1)	-42	+13, 4	$30 - 0.3 \times 22$	3

TABLE Results of Eu¹⁵¹ Mössbauer measurements.

Material	I. S. at 78 K (versus EuF ₃ at 78 K, mm/sec)	H _{int} at 4.2 K (kG)	Magnetic ordering temp. (K)
EuRh ₂	+2.48 ± 0.04	0	(0)
EuRh ₂ H _x	-10.82 ± 0.04	269 ± 3	15.5 ± 0.5
EuPd	-8.12 ± 0.04	160 ± 2	48 ± 2
EuPdH _x	-11.20 ± 0.04	264 ± 3	21 ± 0.5
EuH ₂	-11.4 ± 0.3 ^b	303 ± 5	16.2 ± 0.05

Applications



Multilayer with magnetically dead-layers

Application to H-inserted Fe/V and Fe/Cr multilayers

B. Hjörvarsson, H. Zabel et al

Dead layers in terms of Fe-Fe interlayer magnetic couplings

Applications

AB : FeTi - FeTiH₁ (orth) – FeTiH_{1.8} (mon.)

H. Wernick et al

**localisation of H atoms (4Ti-2Fe) octahedra
impact of the lattice distortion
diffusion coefficient, from line broadening**

AB₂ : Zr(Fe,Co)₂ and Zr(Fe,Co)₂H_x with 0 < x < 4

L. Ferreira et al

**location of H atoms (2Zr-2M) tetrahedra
diffusion process with temperature
local weak magnetic polarisation related to
mobility of H**

R₆Mn₂₃ : Gd₆Mn₂₃ – Gd₆Mn₂₃H_x with 0 < x < 30

G. Long W. Yelon et al.

**location of H in a 4-5 site model
change in the magnetic ordering due to the
depleting of the valence band**

Perturbed angular correlation of gamma rays (PAC)

PAC is used to resolve different local environments of probe atoms in solids. Internal fields in solids exert torques on nuclear moments: an internal magnetic field exerts a torque on the magnetic dipole moment and an internal electric-field gradient exerts a torque on the electric quadrupole moment. These so-called **nuclear hyperfine interactions** lead to frequencies of rotation of probe nuclei that are proportional to the internal fields.

Many PAC probes have an excited nuclear state reached through a gamma-gamma cascade. **Start** and **stop** gamma ray signal creation and decay of the nuclear state. In general, there is an angular correlation between directions of emission of the two gamma rays. Such is the case, for example, following decay of ^{60}Co , for which the lifetime of the intermediate nuclear state is very short. However, when the state lives long enough for the nuclear spin to precess through an appreciable angle, the interaction frequency can be measured with good precision. The number of good PAC probes is limited: probes having favorable nuclear parameters are ^{111}In , decaying into ^{111}Cd , and ^{181}Hf , decaying into ^{181}Ta .

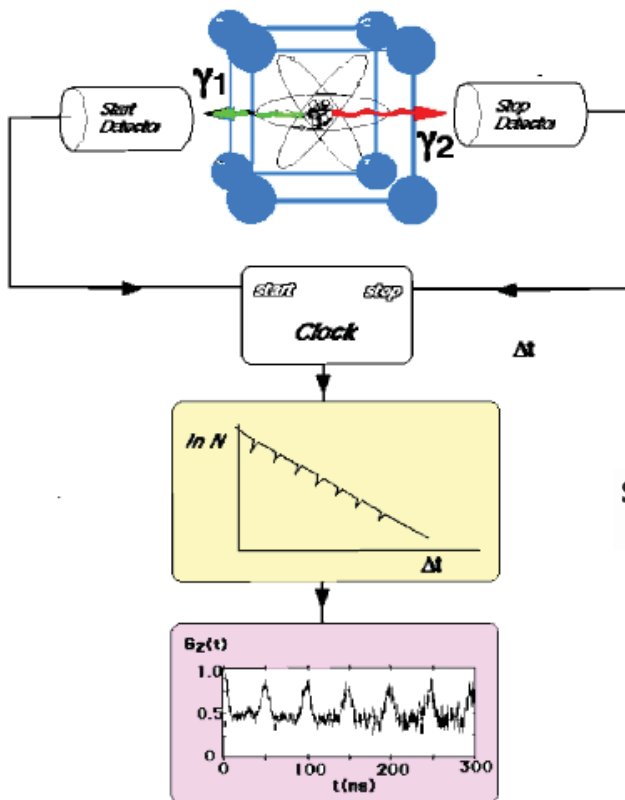
Internal fields are produced mainly by charges and spins within the closest few atomic shells. More distant charges and spins only contribute to inhomogeneous broadening of fields from nearby shells. As a result, **interaction frequencies can be used to characterize the different local atomic environments in which probe atoms find themselves**. Once a frequency has been identified with an underlying environment, it can be recognized in studies made after other methods of preparation.

The Method

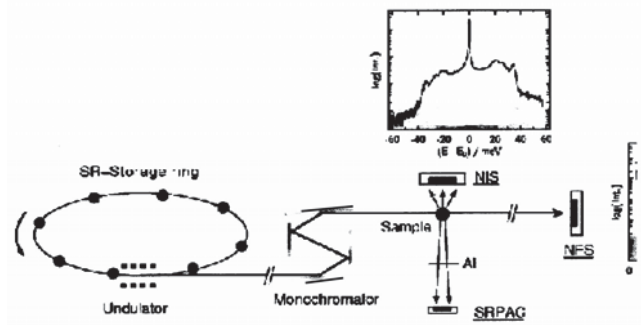
The graphic below gives an impression of PAC spectroscopy. At top is a crystalline sample containing a radioactive probe atom. Emission of **start** and **stop** gamma rays signal formation and decay of the intermediate PAC nuclear state and are detected in scintillation detectors. A clock and histogramming memory records time intervals between start and stop gamma rays, that is, the distribution of individual nuclear lifetimes. The measured distribution is a lifetime decay curve modulated by spin precessions of the nuclei. The modulation, or **perturbation, function $G_2(t)$** contains all information about the internal fields in the sample.

Applications

- phase transformations; multiphase analysis
- structural and magnetic phase transitions: critical behavior and exponents
- magnetism: spin dynamics, stability of atomic magnetic moments in different hosts, exchange interactions, thin film and multilayered materials
- diffusion and other atom movement in solids, dynamical interactions
- surfaces and interfaces: nanocrystals
- point defects: types, thermodynamic properties, interactions, radiation and implantation damage



Synchrotron Radiation-based Perturbed Correlation



Nuclear Forward Scattering

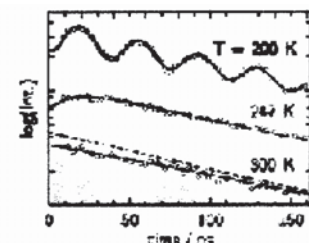
Static and dynamic hyperfine interactions

Nuclear Inelastic Scattering

Partial density of phonons

SR-PAC

Nuclear resonant scattering of synchrotron radiation: Scattering geometries measurements with NFS, NIS and SRPAC.



Applications

AB_2 : $Zr(Fe,Co)_2$ and $Zr(Fe,Co)_2H_x$ with $0 < x < 4$

J. Ayres de Campos et al

location of H atoms (2Zr-2M) tetrahedra
diffusion process with temperature

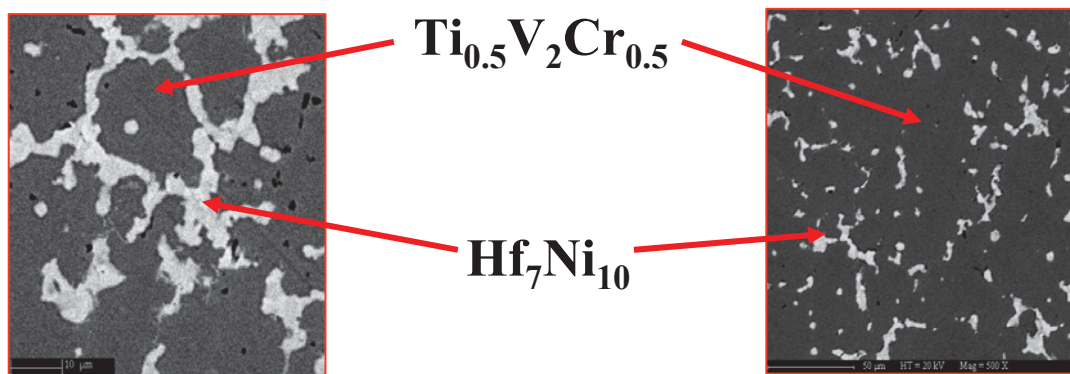
local weak magnetic polarisation related to
mobility of H

TiVCr (BCC) and TiVCr hydrides reveal excellent
so-called «catalysts» to activate the hydrogenation/
dehydrogenation kinetics $Mg \leftrightarrow MgH_2$ (ball-milling)

In fact ~5% addition of $Zr(Hf)_7Ni_{10}$ improves markedly
the activity of the TiCrV based composite alloy.

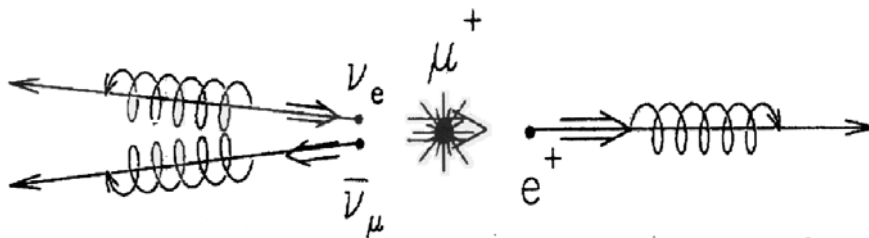
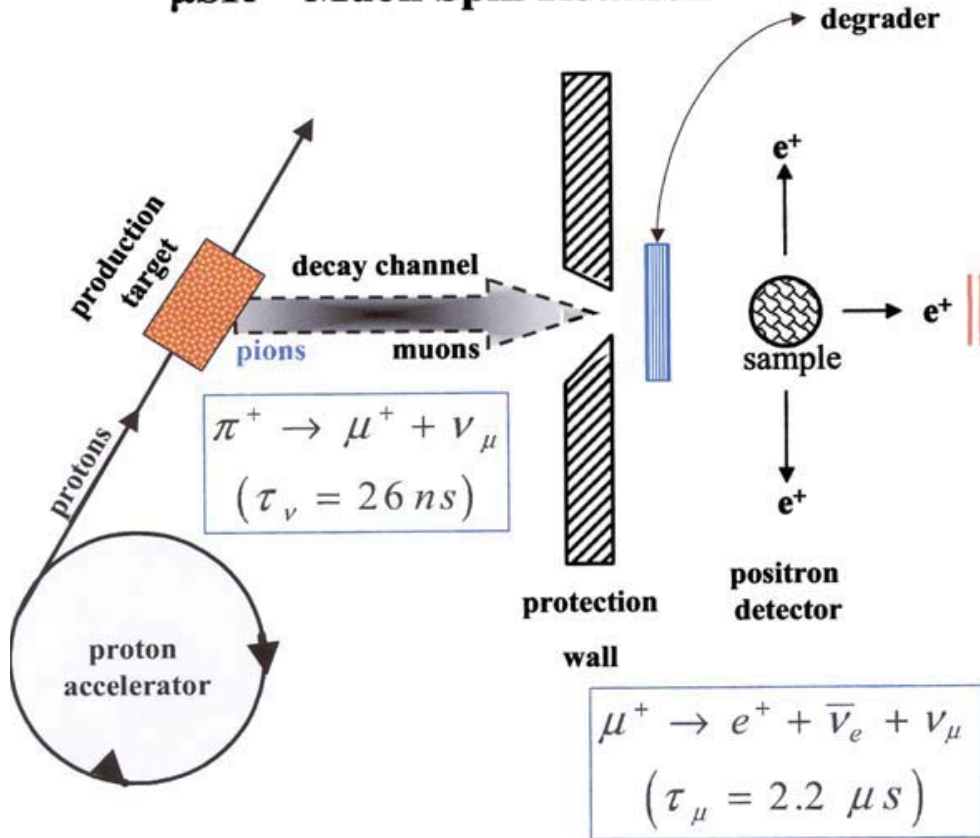
PAC analysis of Hf_7Ni_{10} and 5% Hf_7Ni_{10} doped-TiVCr
demonstrates a marked synergic effect at the grain
boundary for a fast hydrogen diffusion in the composite
alloys.

J. Gil et al

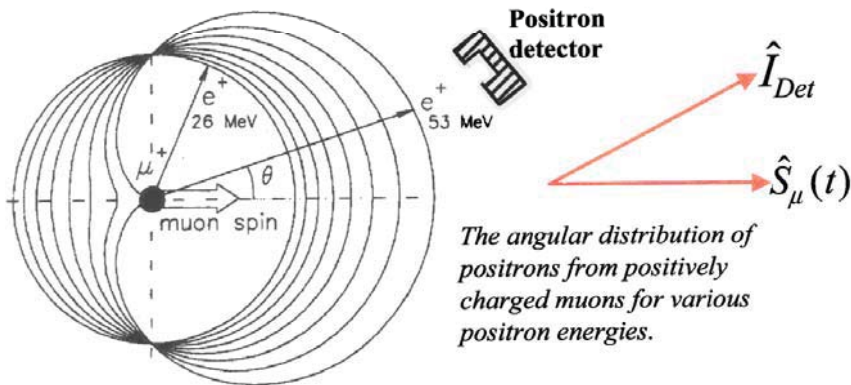


Muon spectroscopy (μ SR)

μ SR Muon Spin Rotation

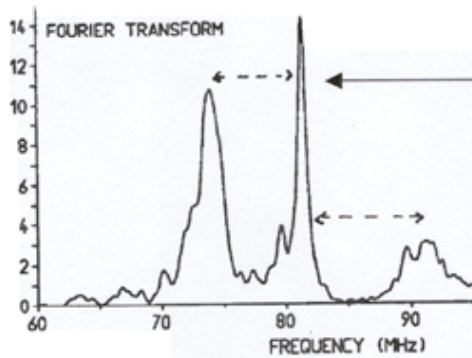
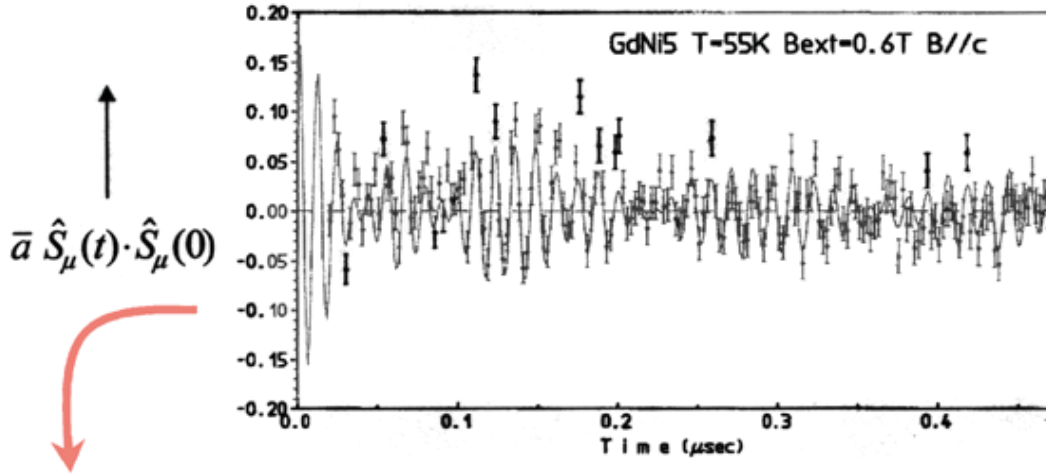


Positive muon decay; this example gives the highest positron energy and an 'asymmetry' of 100%, i.e. the positron has zero probability of being emitted opposite to the muon spin vector. The half-life for muon decay is 2.197 μ s



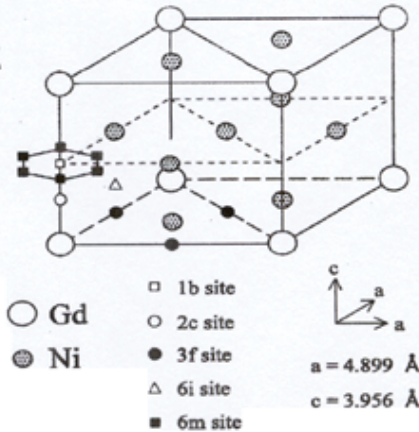
Applications

Constant \vec{B} -Field



Larmor frequency:

$$\omega_L = \gamma_\mu B$$



Hexagonal crystal structure of GdNi₅ (space group P6/mmm). Several interstitial sites are indicated. The muon localizes at the 3f site

By probing the GdNi₅ and GdNi₅H₆, both templates of the well-known LaNi₅H_x systems, magnetic μ^+ SR spectroscopy allows determine preferred location where muons precess and diffuse before their decay.

H. Weidinger

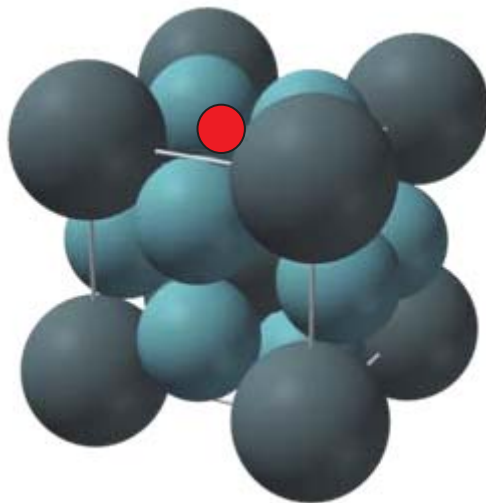
Applications

The A15 materials exhibit interestingly high superconducting temperature e.g. Nb_3Sn ~ 22 K, a base of superconductive wires of cryomagnet coils (e.g. scanner).

Superconductivity has been related to a phonon soft mode that condense down to a pre-martensitic transition.

Hydrogen insertion in V_3Si was proven to destroy very readily the superconducting behaviour. $\mu^+\text{SR}$ spectroscopy was used to demonstrate the local impact on the electric field gradient, leading to modify enough the conditions to stabilise a soft Mode and superconductivity.

H. Weidinger, A Yaouanc et al



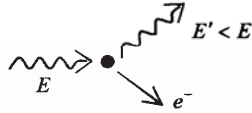
X-ray Absorption

Summary: interactions of X-rays with matter

- elastic scattering
(Thompson or Rayleigh scattering)



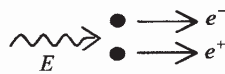
- inelastic scattering
(Compton scattering)



- photoelectric absorption



- pair creation

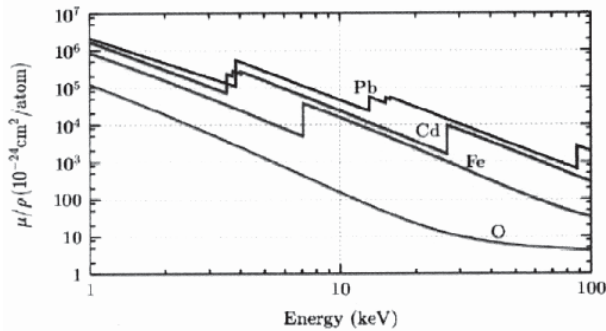
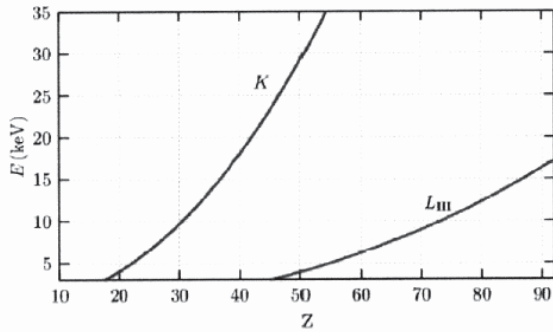
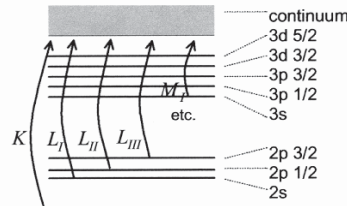


Understanding X-ray absorption is important for

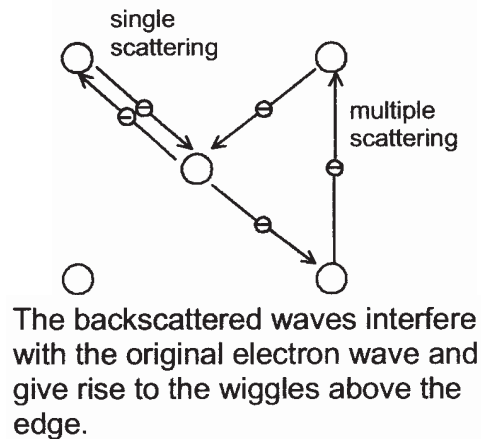
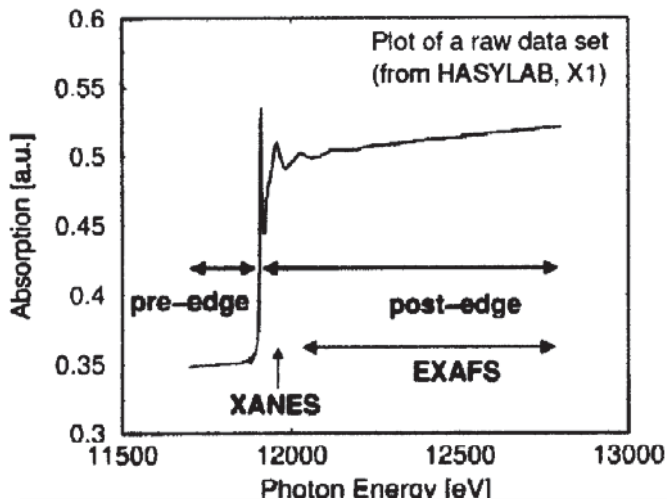
- X-ray radiography (e.g. medical X-rays, baggage screening)
- accurate description of X-ray diffraction ("dispersion corrections", "anomalous scattering")
- absorption spectroscopy (e.g. identification of elements and valence states in materials)

$\hbar\omega < 100 \text{ keV}$	photoelectric absorption dominates
$100 \text{ keV} < \hbar\omega < 1 \text{ MeV}$	Thompson and Compton scattering dominate
$\hbar\omega \gtrsim 1 \text{ MeV} (= 2m_e c^2)$	pair production dominates

In the regime dominated by photoelectric absorption, there are prominent "absorption edges" characteristic of the binding energies of electrons in specific atoms (or ions).

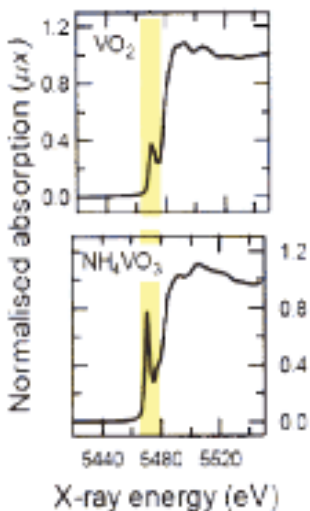


Absorption edges and mass attenuation coefficients for various elements



The "X-ray absorption near edge structure" (XANES) is due to transitions into unoccupied bound states below the edge of the continuum. The "Extended X-ray absorption fine structure" (EXAFS) above the edge is due to backscattering of the photoelectron to the emitting atom:

XANES at V K-edge



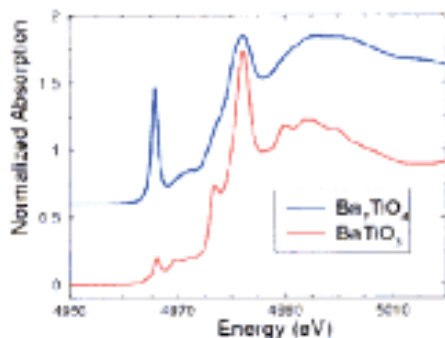
nearly octahedral coordination

Centrosymmetry, no pd mixing, only quadrupole transitions

nearly tetrahedral coordination

Strong pd-mixing, dipole transitions contribute to pre-edge structure

XANES at Ti K-edge



tetrahedral

octahedral

NMR

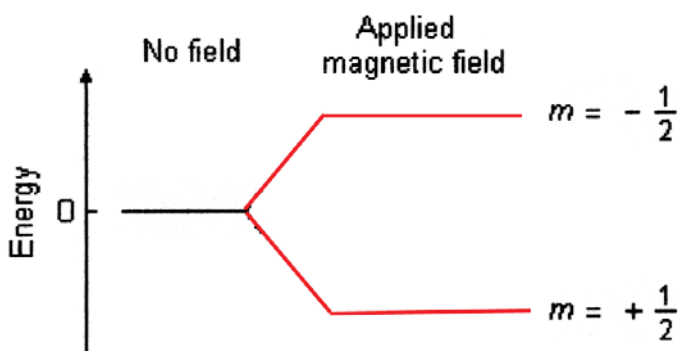
Nuclear spin and the splitting of energy levels in a magnetic field

Subatomic particles (electrons, protons and neutrons) can be imagined as spinning on their axes. In many atoms (such as ^{12}C) these spins are paired against each other, such that the nucleus of the atom has no overall spin. However, in some atoms (such as ^1H and ^{13}C) the nucleus does possess an overall spin. The rules for determining the net spin of a nucleus are as follows;

1. If the number of neutrons **and** the number of protons are both even, then the nucleus has **NO** spin.
2. If the number of neutrons **plus** the number of protons is odd, then the nucleus has a half-integer spin (i.e. $1/2, 3/2, 5/2$)
3. If the number of neutrons **and** the number of protons are both odd, then the nucleus has an integer spin (i.e. 1, 2, 3)

The overall spin, I , is important. Quantum mechanics tells us that a nucleus of spin I will have $2I + 1$ possible orientations. A nucleus with spin $1/2$ will have 2 possible orientations. In the absence of an external magnetic field, these orientations are of equal energy. If a magnetic field is applied, then the energy levels split. Each level is given a *magnetic quantum number*, m .

Energy levels for a nucleus with spin quantum number $1/2$



Magnetic Moment
Energy

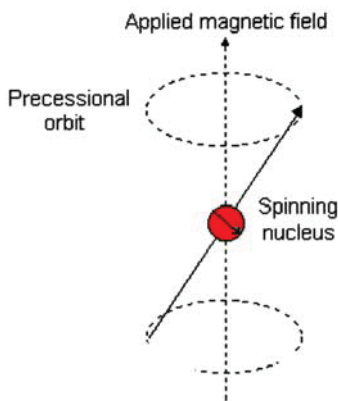
$$\mu = \frac{\gamma I \hbar}{2 \pi}$$

Energy Level

$$E = - \frac{\gamma \hbar}{2 \pi} m B$$

Transition

$$\Delta E = \frac{\gamma \hbar B}{2 \pi}$$



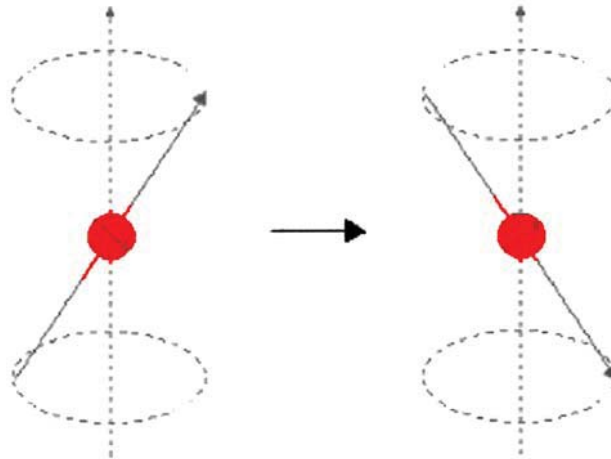
The frequency of precession is termed the *Larmor frequency*, which is identical to the transition frequency.

The potential energy of the precessing nucleus is given by;

$$E = -\mu B \cos \theta$$

where θ is the angle between the direction of the applied field and the axis of nuclear rotation.

If energy is absorbed by the nucleus, then the angle of precession, θ , will change. For a nucleus of spin $1/2$, absorption of radiation "flips" the magnetic moment so that it **opposes** the applied field (the higher energy state)



It is important to realise that only a small proportion of "target" nuclei are in the lower energy state (and can absorb radiation). There is the possibility that by exciting these nuclei, the populations of the higher and lower energy levels will become equal. If this occurs, then there will be **no** further absorption of radiation. The spin system is *saturated*. The possibility of saturation means that we must be aware of the relaxation processes which return nuclei to the lower energy state.

Two major relaxation processes

Spin-lattice (logitudinal) relaxation : T1 (g and mobility)

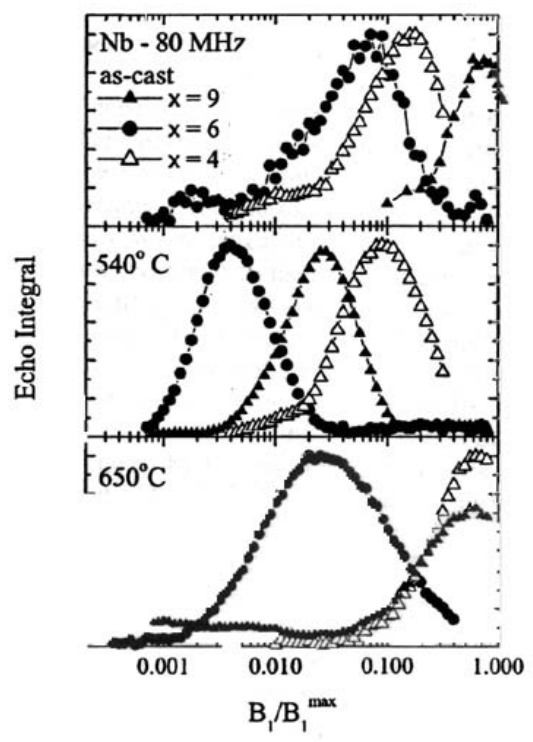
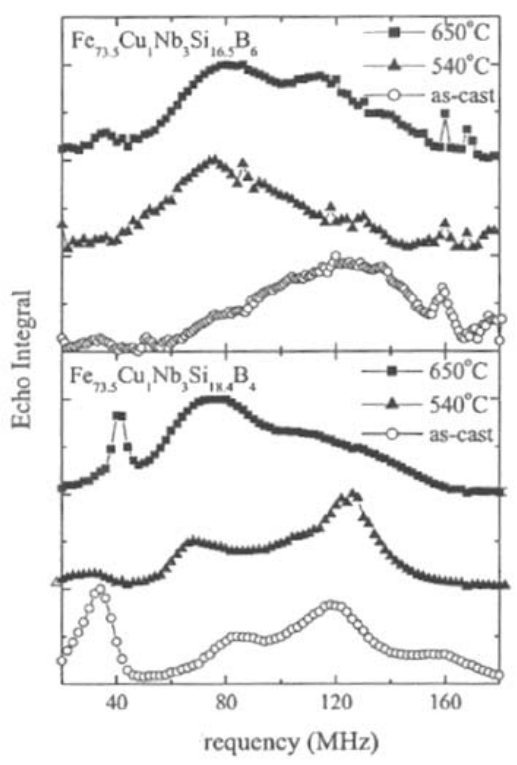
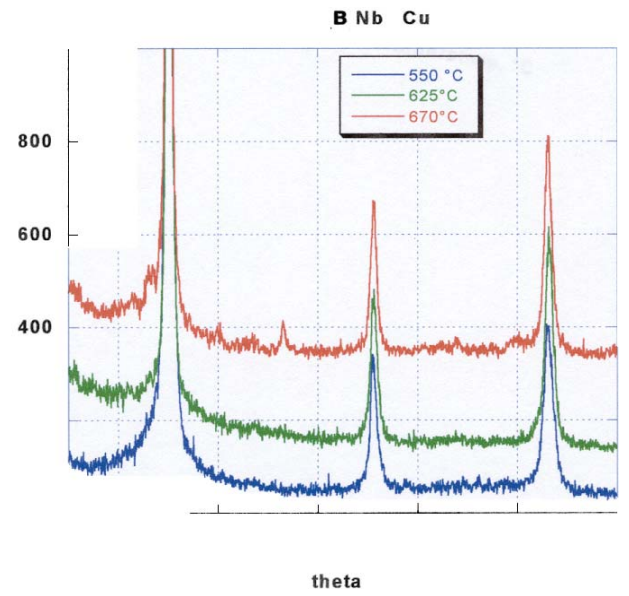
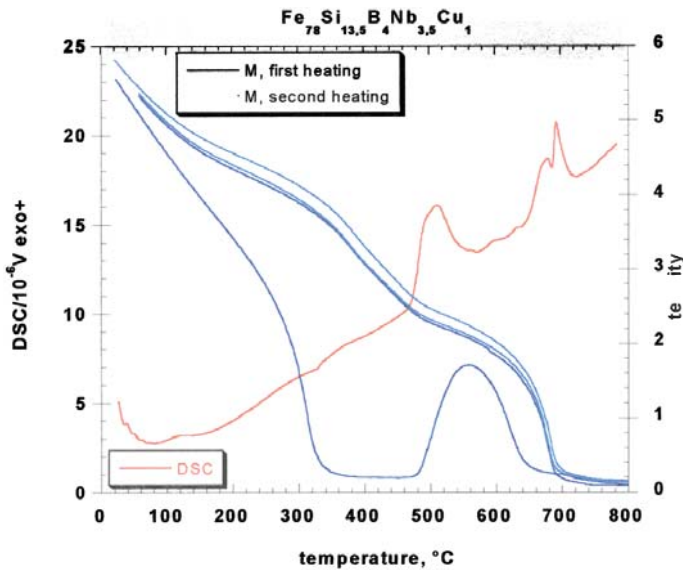
Spin-spin (transverse) relaxation : life-time (coupling)

broadening

Chemical Shift : electron nuclear-shielding

Spin –Spin coupling : e.g. molecular systems

Phase transitions in glassy metals - magnetic trends



NMR spectra for $Fe_{73.5}Cu_1Nb_3Si_{(22.5-x)}B_x$ melt-spun ribbons with $x = 4$ and 6 , measured for different annealing temperatures, at 4.2 K and zero applied magnetic field. The crystallization kinetics evolves from bottom to top.

Spin echo amplitude as a function of the relative power of the rf field B_1/B_1^{max} , taken at approximately 80 MHz (^{93}Nb resonance), for as-cast and annealed melt-spun ribbons of $Fe_{73.5}Cu_1Nb_3Si_{(22.5-x)}B_x$ with $x = 4, 6$ and 9 .

Experimental methods for measuring the diffusion of hydrogen in metals

Method	Property measured
1. Permeation Absorption - Desorption	Diffusivity Solubility
2. Electrochemical method	Diffusivity Solubility
3. Resistivity relaxation	Diffusivity
4. Quench-recovery method	Diffusivity
5. Mechanical relaxation	
a) Gorsky effect	Diffusivity
b) Snoek effect	Jump frequency
c) Internal friction	Jump frequency
6. Magnetic disaccommodation	Jump frequency
7. NMR and related methods	
a) NMR	
Relaxation time	Jump frequency
Pulsed field gradient	Diffusivity
b) μ SR	Jump frequency
c) Mössbauer effect	Jump frequency
d) Perturbed angular correlation	Jump frequency
8. Quasi-elastic neutron scattering (QNS)	
$Q \sim 1/a$	Jump frequency
	Path
$Q < 1/a$	Diffusivity

To investigate solid state materials

e.g. Intermetallics – Metal Hydrides (Magnetics)

**many fully complementary and performing
techniques**

reveals performing such as

Neutron Scattering

Elastic / Inelastic – Coherent / Incoherent

Absorption Edge X-rays Spectroscopies

XANES – Edge – EXAFS – XMCD

as well as

Mössbauer – PAC - Muon Spectr., NMR

those providing very various scales of windows

on the chemical and physical properties

Neutron & synchrotron scattering facilities



ESRF (Synchrotron)



Thank you very much
for your kind attention